

Quantum Phase Diagrams of Matter-Field Hamiltonians II: Wigner Function Analysis

R. López-Peña, S. Cordero, E. Nahmad-Achar, O. Castaños

Instituto de Ciencias Nucleares, Universidad Nacional Autónoma de México,
Apartado Postal 70-543, 04510 Cd. Mx., Mexico

E-mail: lopez@nucleares.unam.mx

Abstract. Non-classical states are of practical interest in quantum computing and quantum metrology. These states can be detected through their Wigner function negativity in some regions. In this paper, we calculate the ground state of the three-level generalised Dicke model for a single atom and determine the structure of its phase diagram using a fidelity criterion. We also calculate the Wigner function of the electromagnetic modes of the ground state through the corresponding reduced density matrix, and show in the phase diagram the regions where entanglement is present. A finer classification is proposed for the continuous phase transitions.

1. Introduction

The Wigner function was introduced in 1932 to give a description of a quantum system in phase space [1]. For some excellent reviews see [2–4]. Its description of a quantum system is complete in the sense that it allows for the calculation of all the quantities that the usual wave function gives, thus supplying all the information of the system in phase space. It is not a real distribution function in phase space because it can be negative, which precludes an ordinary probability interpretation. The initial importance of the Wigner function was that it allowed to treat quantum mechanics and thermodynamics on the same footing as their classical counterparts, making it easier to identify new effects in the quantum case. One of the first areas to adopt the Wigner function was that of optics, where it was employed to describe the coherence and the polarisation of optical fields [5], to explore the quantum effects in electron transport [6], to investigate the transport in resonant tunneling devices [7–9], to study wave propagation through media [10], to inquire into different theories of quantum dissipation [11], etc.

The concept of entanglement, on the other hand, emerges with the Einstein-Podolsky-Rosen paradox [12], although it was Schrödinger who coined the term [13]. In it, the nonlocal behaviour of the system is reflected in the correlation between distant points, which the Wigner function visually displays. When this occurs, negative values in the function appear as a consequence of the interference between distant regions in

phase space [14]; for this reason the volume of the negative part of the Wigner function has been proposed as a measure of non-classicality of quantum states [15].

Experimentally, the Wigner function for quantum optical systems can be reconstructed using homodyne tomography [16], field ionisation detectors [17, 18], photon-counting [19], two-window heterodyne measurements [20], etc. For non-separable laser beams through a toroidal mirror see [21]. For other classes of systems it can also be determined: one can mention two Bell states and the five-qubit Greenberger-Horne-Zeilinger (GHZ) spin Schrödinger cat state [22]; a single harmonically trapped atom [23]; an ensemble of helium atoms formed by partially coherent illumination of a double slit [24], etc. This has practical importance in quantum information processing, because the Wigner function provides more information about the quantum system than any other quantum approach [25].

In this work, we analyse the behaviour in phase space of the two radiation modes of light along the finite phase diagram of the ground state of the Hamiltonian describing a single three-level atom interacting dipolarly with two radiations modes in a cavity; to this end, we calculate the Wigner function of the radiation modes for different points of the space parameters to depict the behaviour of the system. The phase transitions are determined and vividly shown in phase space, validating the separatrices obtained through the fidelity criterion given in [26]. The numerical expressions given for the Wigner function enable us to calculate the expectation values of all the observables for the corresponding electromagnetic mode. A finer classification is also proposed for the continuous phase transitions, which may clearly be seen through the Wigner function.

In section II we introduce the generalisation of the Dicke model to describe the system. In section III we explain how we use the fidelity to calculate the quantum phase transitions in parameter phase space. Section IV shows how the Wigner function is calculated, and in section V we show the results obtained. Finally in section VI we give a summary and conclusions.

2. Dicke Generalised Models

We consider the multipolar Hamiltonian for the dipole interaction between a two-mode radiation field and a 3-level atomic system in the long wave approximation, which may be written as [27–29] ($\hbar = 1$)

$$\mathbf{H} = \mathbf{H}_D + \mathbf{H}_{int} , \quad (1)$$

where \mathbf{H}_D is the diagonal matter and field independent contributions,

$$\mathbf{H}_D = \sum_{j < k}^3 \Omega_{jk} \mathbf{a}_{jk}^\dagger \mathbf{a}_{jk} + \sum_{j=1}^3 \omega_j \mathbf{A}_{jj} , \quad (2)$$

and \mathbf{H}_{int} is the matter-field dipolar interaction

$$\mathbf{H}_{int} = -\frac{1}{\sqrt{N_a}} \sum_{j < k}^3 \mu_{jk} (\mathbf{A}_{jk} + \mathbf{A}_{kj}) (\mathbf{a}_{jk} + \mathbf{a}_{jk}^\dagger) . \quad (3)$$

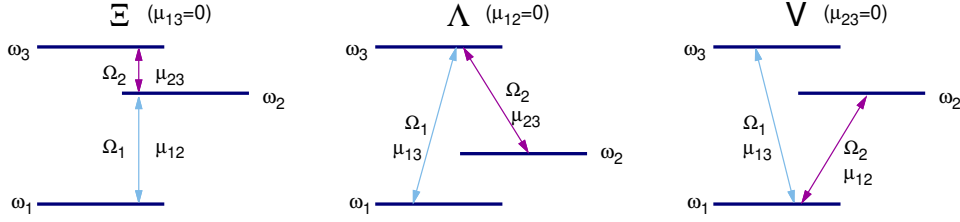


Figure 1. 3-level atomic configurations. The i -th atomic energy level ($\hbar = 1$) is denoted by ω_i , and the coupling parameter between levels i and j is μ_{ij} . The field frequencies are denoted by Ω_{ij} . A particular atomic configuration is obtained by choosing appropriately the vanishing dipolar strength μ_{jk} in eq.(3): for Ξ we take $\mu_{13} = 0$, for Λ we take $\mu_{12} = 0$, and for V we take $\mu_{23} = 0$.

Here, N_a denotes the number of particles, \mathbf{a}_{jk}^\dagger , \mathbf{a}_{jk} are the creation and annihilation photon operators for the mode Ω_{jk} which promotes transitions between the atomic levels ω_j and ω_k , and \mathbf{A}_{ij} are the matter operators obeying the $U(3)$ algebra

$$[\mathbf{A}_{ij}, \mathbf{A}_{lm}] = \delta_{jl} \mathbf{A}_{im} - \delta_{im} \mathbf{A}_{lj} , \quad (4)$$

with $\sum_{k=1}^3 \mathbf{A}_{kk} = N_a \mathbf{I}_{\text{matter}}$. The coupling parameter between levels ω_j and ω_k has been denoted by μ_{ij} , and we have assumed that the atomic frequencies satisfy $\omega_1 \leq \omega_2 \leq \omega_3$. We also fix $\omega_1 = 0$. Note that a particular atomic configuration is obtained by making an appropriate dipolar strength μ_{ij} to vanish (cf. Fig. 1).

A variational study which involves coherent states for both matter and field contributions, provides a good approximation of the ground state energy surface per particle. The phase diagram in this approach shows the normal and collective regions, the latter divided into (two) regions where only one kind of photon contributes to the ground state, while the former remains in the vacuum state [28]. This signature of the phase diagram remains when the symmetries of the Hamiltonian are restored in the variational solution and the thermodynamic limit is taken [30]. In figure 2 the phase diagram and energy surface as functions of the dimensionless strengths x_{jk} ($x_{jk} = \mu_{jk}/\mu_{jk}^c$ with μ_{jk}^c the critical value of the corresponding two level system) for the three atomic configuration are given, the separatrix (points where a sudden change in the ground state composition takes place) is draw in white lines, and the order of the transitions (using the Ehrenfest classification [31]) is shown. In the normal region (in black), labeled as N and where atoms emit and absorb independently, both photons are in the vacuum state and the matter contribution is in its lowest energy state; while in the collective regions (gradient coloured regions), labeled as S_{jk} and where superradiance takes place, only photons of kind Ω_{jk} and atomic populations in the levels ω_j and ω_k have non-zero contribution.

An exact calculation of the ground state involves a numerical diagonalisation of the Hamiltonian matrix. The Hamiltonian (1) is invariant under parity transformations of the form

$$\Pi_1 = e^{i\pi \mathbf{K}_1} , \quad \Pi_2 = e^{i\pi \mathbf{K}_2} , \quad (5)$$

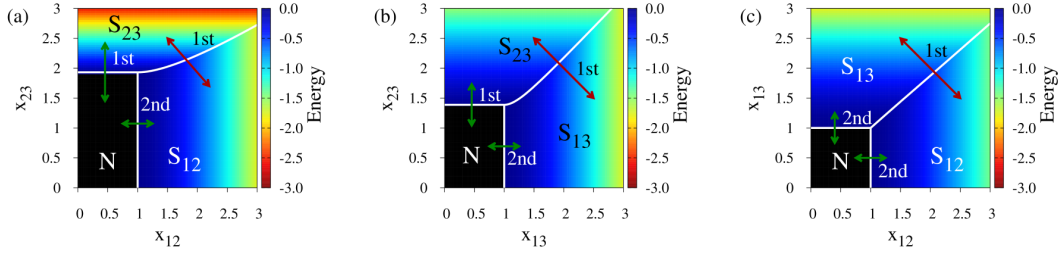


Figure 2. (colour online) Phase diagrams and energy surfaces, per particle, for the variational solution (thermodynamic limit) in the (a) Ξ -configuration with $\omega_2/\omega_3 = 1/3$, (b) Λ -configuration with $\omega_2/\omega_3 = 1/10$, and (c) V -configuration with $\omega_2/\omega_3 = 8/10$. The separatrices (white lines) and the order of the transitions are shown. The Normal regions (in black) are labeled by N . The superradiant regions divide themselves into subregions denoted by S_{ij} , where mode Ω_{ij} dominates. In all cases matter and field are in resonance, and the axes are $x_{ij} = \mu_{ij}/\mu_{ij}^c$, where μ_{ij}^c is the 2-level critical coupling. In this and other plots, the energy is measured in units of $[\hbar\omega_3]$ and x_{ij} is dimensionless.

Table 1. Coefficients $\eta_{ij}^{(s)}$ and $\lambda_k^{(s)}$ corresponding to the operators \mathbf{K}_s in eq. (6) are given for the atomic Λ -, Ξ - and V -configurations.

Conf.	\mathbf{K}_s	$\eta_{12}^{(s)}$	$\eta_{13}^{(s)}$	$\eta_{23}^{(s)}$	$\lambda_1^{(s)}$	$\lambda_2^{(s)}$	$\lambda_3^{(s)}$
Λ	\mathbf{K}_1	0	1	1	0	0	1
	\mathbf{K}_2	0	0	1	1	0	1
Ξ	\mathbf{K}_1	1	0	1	0	1	2
	\mathbf{K}_2	0	0	1	0	0	1
V	\mathbf{K}_1	1	1	0	0	1	1
	\mathbf{K}_2	0	1	0	0	0	1

where \mathbf{K}_s , $s = 1, 2$, are constants of motion when the rotating wave approximation (RWA) is taken, which are found through the conditions $[\mathbf{\Pi}_j, \mathbf{H}] = 0$. Assuming that \mathbf{K}_s is a linear operator, we find

$$\mathbf{K}_s = \eta_{12}^{(s)} \boldsymbol{\nu}_{12} + \eta_{13}^{(s)} \boldsymbol{\nu}_{13} + \eta_{23}^{(s)} \boldsymbol{\nu}_{23} + \sum_{k=1}^3 \lambda_k^{(s)} \mathbf{A}_{kk} . \quad (6)$$

where $\boldsymbol{\nu}_{12}$, $\boldsymbol{\nu}_{13}$, and $\boldsymbol{\nu}_{23}$ denote the number of photons of each electromagnetic field mode. The coefficients $\eta_{ij}^{(s)}$ and $\lambda_k^{(s)}$ of the operators are given in table 1 for the different atomic configurations. The operators shown \mathbf{K}_s were chosen as linear combinations of constants of motion with non-negative integer eigenvalues.

Accordingly, the Hilbert space \mathcal{H} divides naturally into four subspaces of the form

$$\mathcal{H} = \mathcal{H}_{ee} \oplus \mathcal{H}_{eo} \oplus \mathcal{H}_{oe} \oplus \mathcal{H}_{oo} ,$$

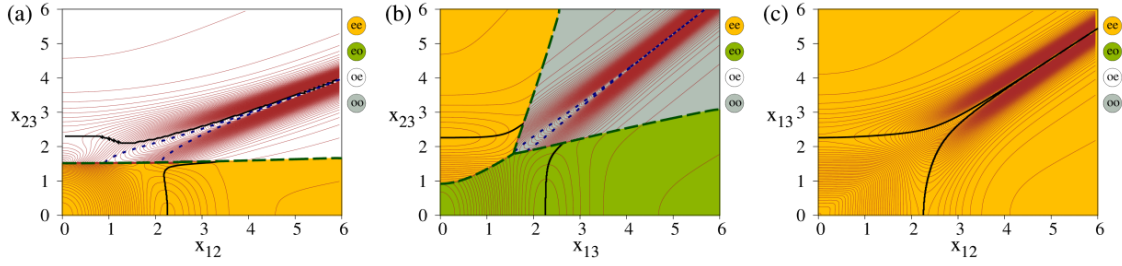


Figure 3. (colour online) Quantum separatrix for a single 3-level atom interacting dipolarly with two modes of electromagnetic field. (a) Ξ -configuration with parameters $\Omega_{12} = 1/4$, $\Omega_{23} = 3/4$ and $\omega_2 = 1/4$. (b) Λ -configuration with parameters $\Omega_{13} = 1$, $\Omega_{23} = 9/10$, and $\omega_2 = 1/10$. (c) V -configuration with parameters $\Omega_{12} = 4/5$, $\Omega_{13} = 1$ and $\omega_2 = 4/5$. In all case we have fixed $\omega_1 = 0$ and $\omega_3 = 1$.

where the subscripts $\sigma = \{ee, eo, oe, oo\}$ denote the even e or odd o parity of Π_1 and Π_2 , respectively.

We use basis states labeled by $|\nu_{12}, \nu_{13}, \nu_{23}\rangle \otimes |n_1, n_2, n_3\rangle$ with $n_1 + n_2 + n_3 = N_a$ and $\nu_{jk} = 0, 1, \dots, \infty$. Because in our model a system of 3-level atoms interacting with a 2-mode field in a cavity generates an infinite dimensional Hilbert space, we need a truncation criterion to study the eigensystem of the Hamiltonian. For this purpose, we request convergence of the fidelity between base states $|\psi(k_{1max}, k_{2max})\rangle$ and $|\psi(k_{1max} + 2, k_{2max} + 2)\rangle$, where (k_{1max}, k_{2max}) are the maximum eigenvalues taken by the operators \mathbf{K}_1 and \mathbf{K}_2 in the current approximation. For the purposes of this work, we choose this convergence to be good when we reach an error of the order $e_{rr} = 10^{-10}$, i.e.,

$$1 - \mathcal{F}(k_1, k_2) \leq 10^{-10} . \quad (7)$$

where $\mathcal{F}(k_1, k_2) = |\langle \psi(k_1, k_2) | \psi(k_1 + 2, k_2 + 2) \rangle|^2$ is the fidelity between the states. This fidelity constraint may be set according to the problem to be approached. We choose the approximation given in Eq. (7) because it allows an approximation of the expectation value of the energy of the ground state good up to 10^{-8} [32, 33], even for large values of the coupling constants. So, in each Hilbert subspace \mathcal{H}_σ , the truncated basis \mathcal{B}_σ is formed by the set of states $|\nu_{12}, \nu_{13}, \nu_{23}\rangle \otimes |n_1, n_2, n_3\rangle$ with all eigenvalues $k_1 \leq k_{1max}$ and $k_2 \leq k_{2max}$ of the operators \mathbf{K}_1 and \mathbf{K}_2 respectively, and which preserve the parity σ . The basis \mathcal{B}_σ obtained in this form will be called the *exact basis*.

3. Fidelity as Signature of Quantum Phase Transitions

Traditionally, to determine the quantum phase transitions in the limit $N_a \rightarrow \infty$, one uses a variational test function and calculates the associated ground state energy surface. This is an analytic function depending on parameters and variables which allows the calculation of its minimum critical points. Those associated to the so-called degenerate critical points determine the locus of points in parameter space where the ground state

suffers a sudden change in its properties. Additionally, one can use the Ehrenfest classification, which determines the order of the quantum phase transitions according to the order of the derivative of the energy surface where the analyticity is lost [34].

Here we are considering *finite* quantum systems, that is, systems with a finite number of particles. The ground state energy is calculated by means of the diagonalisation of the corresponding Hamiltonian matrix, and in order to determine the regions where a sudden change in the characteristics or properties of the ground state takes place we use quantum information concepts, such as the fidelity and the susceptibility of the fidelity. We shall here refer to such a change in the behaviour and constitution of the ground state as a quantum phase transition; in the current literature it has also been called a quantum crossover.

The loci where the fidelity between neighbouring states $|\Psi_g(\xi_1)\rangle$, $|\Psi_g(\xi_2)\rangle$ along parametric lines $\xi(t)$ in parameter space

$$\mathcal{F}(\rho_{\xi(t)}, \rho_{\xi(t+\delta)}) = |\langle \Psi_g(\xi(t)) | \Psi_g(\xi(t+\delta)) \rangle|^2 \quad (8)$$

presents a minimum, determine points of the separatrix. For a large number of particles, one may follow trajectories which are parallel to the axes, as all other trajectories will yield the same separatrix (cf. Fig. 2). However, for a finite number of particles, one must consider trajectories in all directions of the plane (x_{ij}, x_{jk}) . Thus, in order to obtain a fine description of the phase diagram we consider the surface of minimum fidelity, calculated by considering neighbouring points in directions parallel to the axes ($x_{jk} = 0$), along identity lines ($x_{ij} = x_{jk}$), and along their orthogonal directions ($x_{ij} = -x_{jk}$), thereby finding the local minima (see Appendix A).

For the three-level systems interacting with two radiation modes in a cavity, in the case of $N_a = 1$ particle, by means of the fidelity and the susceptibility of the fidelity, we have found three types of loci of points where the ground states changes abruptly (cf. figure 3): The dashed lines indicate discontinuous transitions where the fidelity Eq. (8) of neighbouring states falls to zero, indicating that the neighbouring states in question are completely dissimilar. The separatrix in this case borders along orthogonal Hilbert subspaces of different parity. On the other hand (full and dotted lines in the figure), there are situations with $F(\xi) \neq 0$ and it either remains different from zero as N_a increases, or reaches zero in the large N_a limit; these both are continuous transitions which we propose to call *stable* and *unstable* continuous transitions; they can be distinguished by means of the calculation of the Bures distance [35, 36], which measures the difference of two probability densities of the quantum system: if ρ_A and ρ_B are the density matrices of states $|\Psi_A\rangle$ and $|\Psi_B\rangle$, the Bures distance between the states is given by

$$D_B^2(\rho_A, \rho_B) = 2 \left(1 - \sqrt{\mathcal{F}(\rho_A, \rho_B)} \right), \quad (9)$$

where the fidelity may be calculated as

$$\mathcal{F}(\rho_A, \rho_B) = \left[\text{Tr} \sqrt{\sqrt{\rho_A} \rho_B \sqrt{\rho_A}} \right]^2, \quad (10)$$

which reduces to $\mathcal{F}(\rho_A, \rho_B) = |\langle \Psi_A | \Psi_B \rangle|^2$ for pure states.

For the stable continuous transition the value of the Bures distance is smaller than for the unstable continuous transition [26].

The first order quantum phase transitions, according to the Ehrenfest classification, can be always determined by means of the Hellmann-Feynman theorem [37, 38]. These type of transitions are always associated to zero fidelity values, that is, discontinuous transitions. On the other hand, the associated changes in the properties of the ground state of the system will be clearly shown in the calculation of the Wigner quasi-probability distribution function of the two-modes of the electromagnetic field in the cavity. These results distinguish the three types of quantum phase transitions appearing for finite quantum systems, viz., the discontinuous, continuous-stable, and continuous-unstable quantum phase transitions.

For few particles (in this work we consider only 1 particle), we use the exact basis introduced in the previous section to calculate the ground state of the system. In order to obtain each minimum energy surface in phase space we use the fidelity criterion given in Eq. (7), for each pair of symmetry values $k_{1\max}$ and $k_{2\max}$ and comparing these with values up to $(k_{1\max} + 2)$ and $(k_{2\max} + 2)$ (for the exact procedure cf. [32, 33]).

The separatrix for the Ξ -, Λ -, and V -configurations are those shown in Fig. (3), where the parity of the eigenvalues of the operators \mathbf{K}_1 and \mathbf{K}_2 Eq. (6), preserved for each energy surface, is indicated by the coloured region and legend. The shape of the surface of maximum Bures distance for each atomic configuration is found in [Appendix A](#), where the discontinuities and local maxima correspond perfectly with the separatrices in figure 3.

For the Ξ configuration, figure 3(a), we see that the parity of the ground state of the system can have only two possibilities, ee and oe , depending on the values of the coupling parameters x_{ij} . Outside the Normal region, the bi-modal character of light is present because mode Ω_{23} is dominant above the dashed line while below it the mode Ω_{12} is preponderant. The fine classification yields stable-continuous transitions (solid line) in the ee and oe -regions and unstable-continuous transitions (dotted line) in the oe -region.

For the Λ configuration, figure 3(b), the energy surface is formed by three parity regions ee , eo and oo . Stable-continuous transitions (solid lines) occur in the ee - and eo -regions, while unstable-continuous transitions (dotted line) are had in the oo -region.

For the V configuration, figure 3(c), a comparison with its thermodynamic counterpart in Fig. 2 shows clearly the correspondence with the domains where each electromagnetic mode is dominant. The ground energy surface has parity ee , the separatrix (solid line) presents stable-continuous transitions except when the curves coalesce, at which points unstable-continuous transitions occur.

The finer classification of the continuous transitions is more evident through the study of the quasi-probabilities, since this classification is based on whether the bulk of the ground state remains in a sub-basis of the total basis or not. In this work we focus our study on the properties of the Wigner function in the different regions. As the Λ configuration appears to have a richer structure, which we will consider it in what

follows, and in section 5 we will discuss its separatrix at length. The Supplementary Material contains the results for all atomic configurations.

4. Calculation of the Wigner Function

In order to study the quantum phase transitions, we make use of the Wigner function of the electromagnetic modes. In this section we calculate the Wigner function following the procedure outlined in [39]. We denote the Fock basis states for the Λ -configuration by

$$|\nu_{13}, \nu_{23}, n_1, n_2, n_3\rangle, \quad (11)$$

with the first two labels denoting the electromagnetic quanta oscillations number, and the next three the population of the atomic levels, which satisfy $n_1 + n_2 + n_3 = N_a$. For this configuration one has the parity operators $e^{i\mathbf{K}_1\pi}$ and $e^{i\mathbf{K}_2\pi}$ with

$$\mathbf{K}_1 = \boldsymbol{\nu}_{13} + \boldsymbol{\nu}_{23} + \mathbf{A}_{33}, \quad (12)$$

$$\mathbf{K}_2 = \boldsymbol{\nu}_{23} + \mathbf{A}_{11} + \mathbf{A}_{33}, \quad (13)$$

whose eigenvalues we denote by k_1 and k_2 , respectively. We may use these to replace the electromagnetic quanta oscillations numbers,

$$\nu_{13} = k_1 - k_2 + n_1, \quad \nu_{23} = k_2 - n_1 - n_3, \quad (14)$$

and thus denote the ground state of the system as

$$\begin{aligned} |\psi_{\text{gs}}\rangle &= \sum_{k_1, k_2} \sum_{n_1, n_3}^{N_a} C_{k_1, k_2, n_1, n_3} \\ &\times |k_1 - k_2 + n_1, k_2 - n_1 - n_3, n_1, N_a - n_1 - n_3, n_3\rangle \end{aligned}$$

Notice that for the Tavis-Cummings model we do not have the sum over indices k_1, k_2 , as these are associated to constant of the motion. For the Dicke model, although k_1, k_2 are not fixed, their parity is invariant.

The density matrix of the ground state of the system can be calculated from the expression above, and from it the reduced density matrices for the modes ν_{13} and ν_{23} are obtained:

$$\begin{aligned} \varrho_{13} &= \sum_{k_1, k'_1, k_2} \sum_{n_1, n_3} C_{k_1, k_2, n_1, n_3} C_{k'_1, k'_2, n_1, n_3}^* \\ &\times |k_1 - k_2 + n_1\rangle \langle k'_1 - k'_2 + n_1|, \end{aligned}$$

$$\begin{aligned} \varrho_{23} &= \sum_{k_1, k_2, k'_2} \sum_{n_1, n_3} C_{k_1, k_2, n_1, n_3} C_{k'_1, k'_2, n_1, n_3}^* \\ &\times |k_2 - n_1 - n_3\rangle \langle k'_2 - n_1 - n_3|. \end{aligned}$$

In order to calculate the Wigner function of the system, one uses an expression for the Weyl symbol $W_{|n\rangle\langle m|}(q, p)$ of the operator $\rho_{nm} = |n\rangle\langle m|$. Writing the Glauber coherent state in the position representation, one arrives at the normalised expression for the Wigner function

$$W_{\alpha,\beta}(q, p) = \exp\left\{-\frac{|\alpha|^2}{2} - \frac{|\beta|^2}{2}\right\} \times \exp\left\{-z z^* + \sqrt{2}\alpha z^* + \sqrt{2}\beta^* z - \alpha\beta^*\right\}, \quad (15)$$

where we have defined the complex variable $z = q + ip$ and the function is normalised with respect to the volume element $d\mu = dq dp$.

Considering the expansion of the coherent states $|\alpha\rangle$ and $|\beta\rangle$ with respect to Fock states we have

$$W_{\alpha,\beta}(q, p) = e^{-\frac{1}{2}(|\alpha|^2 + |\beta|^2)} \sum_{n,m} \frac{\alpha^n \beta^{*m}}{\sqrt{n! m!}} W_{|n\rangle\langle m|}(q, p).$$

Now, through the generating function for the associated Laguerre polynomials, and some algebra, we arrive at

$$W_{|n\rangle\langle m|}(q, p) = \frac{(-1)^m}{\pi} 2^{\frac{n-m}{2}} \sqrt{\frac{m!}{n!}} (q - ip)^{n-m} \times e^{-(q^2 + p^2)} L_m^{n-m}(2(q^2 + p^2)), \quad (16)$$

for $n \geq m$. For $n < m$ we need to interchange $n \leftrightarrow m$, together with $q - ip \rightarrow q + ip$. In this manner we obtain the Wigner function for the reduced density matrices:

$$W_{13}(q, p) = \sum_{k_1, k_2, k'_1} \sum_{n_1, n_3} C_{k_1, k_2, n_1, n_3} C_{k'_1, k_2, n_1, n_3}^* W_{|k_1 - k_2 + n_1\rangle\langle k'_1 - k_2 + n_1|}(q, p), \quad (17)$$

$$W_{23}(q, p) = \sum_{k_1, k_2, k'_2} \sum_{n_1, n_3} C_{k_1, k_2, n_1, n_3} C_{k'_2, k'_2, n_1, n_3}^* W_{|k_2 - n_1 - n_3\rangle\langle k'_2 - n_1 - n_3|}(q, p). \quad (18)$$

5. Wigner function and quantum phase transitions

In the following figures we illustrate the quantum phase transitions for $N_a = 1$ atom in the Λ -configuration, with the parameters given in Fig. 3. We plot the Wigner function as a function of the quadratures q and p at various points at either side of a separatrix (continuous, dashed and dotted lines in the figures), in order to show how it behaves as the system undergoes a phase transition. Each plot displays W_{13} at the upper right and W_{23} at the upper left, the phase diagram is shown below them, and in it a solid (red) dot marks the point at which the Wigner function is calculated. We also provide, as supplementary material, movies which show, for the three atomic configurations Ξ , Λ , and V , the Wigner function along a trajectory which goes through different regions of the phase diagram crossing the different separatrices.

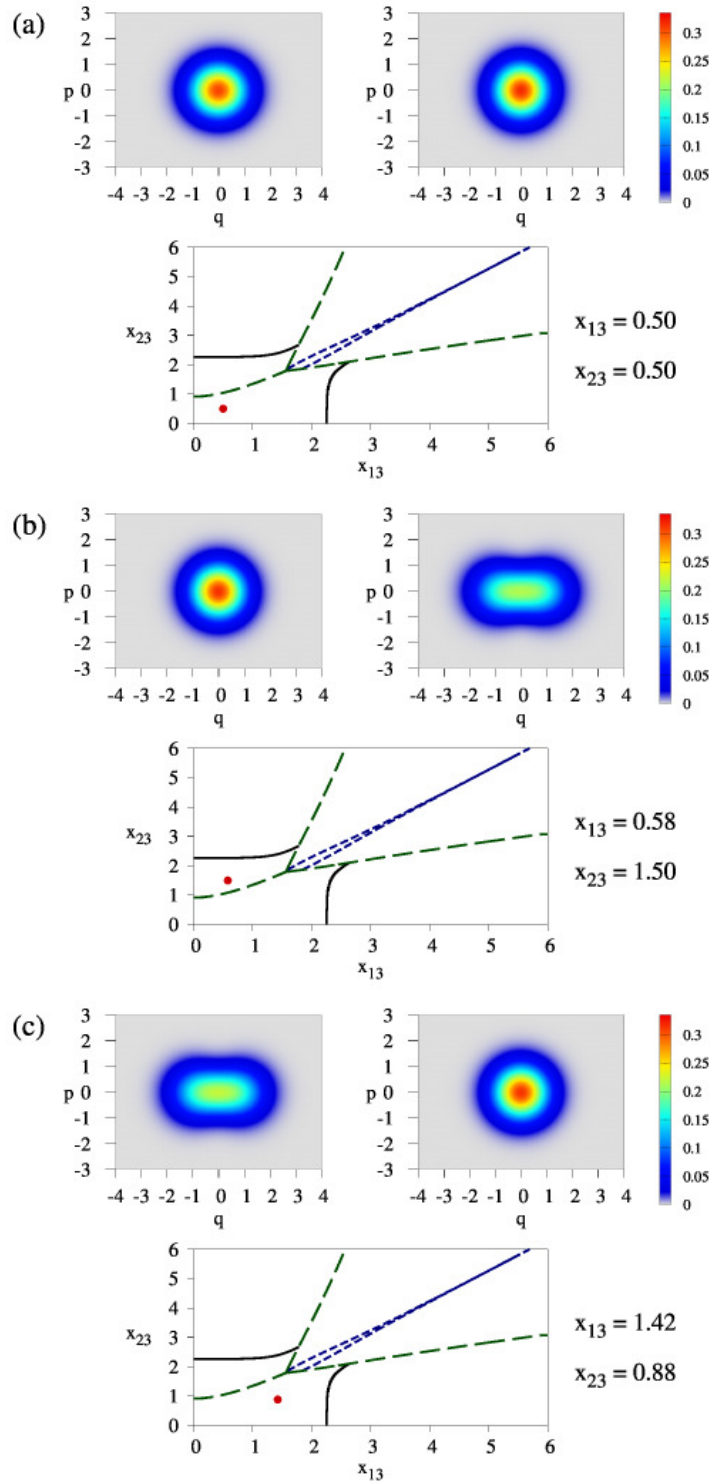


Figure 4. (Colour online) behaviour of the Wigner function in the normal region for (a) a point with small values of both x_{13} and x_{23} , (b) a point in the region $x_{13} < x_{23}$ over the separatrix, and (c) a point the region $x_{13} > x_{23}$ below the separatrix. The values of x_{13} and x_{23} at the point in question (red in the figure) are indicated.

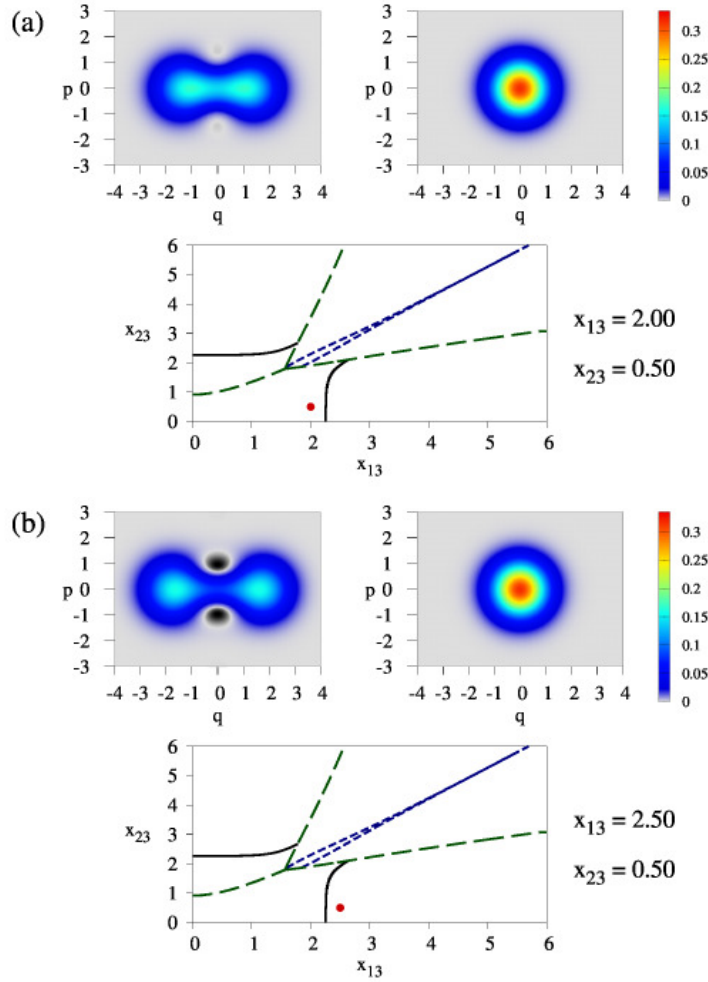


Figure 5. (Colour online) behaviour of the Wigner function as the system goes through a stable-continuous transition.

We first note that the phase diagram for $N_a = 1$ reveals a rich structure not present in the thermodynamic limit of the system. In the thermodynamic limit, there are only three regions present: the normal regime, where the behaviour is not dominated by any of the electromagnetic modes, and two collective regions where one of the electromagnetic modes is prevalent [cf. figure 2(b)]. On the other hand, the phase diagram for $N_a = 1$ divides the parameter space into three regions with fixed parity, each of which in turn splits into at least two regions [cf. figure 3(b)].

In Fig. 4(a), the Wigner functions W_{13} and W_{23} are shown for small values of the parameters x_{13} and x_{23} . Both functions are positive and have circular symmetry, i.e., the bulk of the ground state is dominated by the vacuum state of the field. Notice that the normal region is divided into two regions by a separatrix (dashed line) where a change of parity occurs (discontinuous transition). Thus, it is of interest to consider points above and below this separatrix, at points where the small contribution of the radiation field is not negligible. This is shown in Figs. 4(b) and 4(c). As we move from

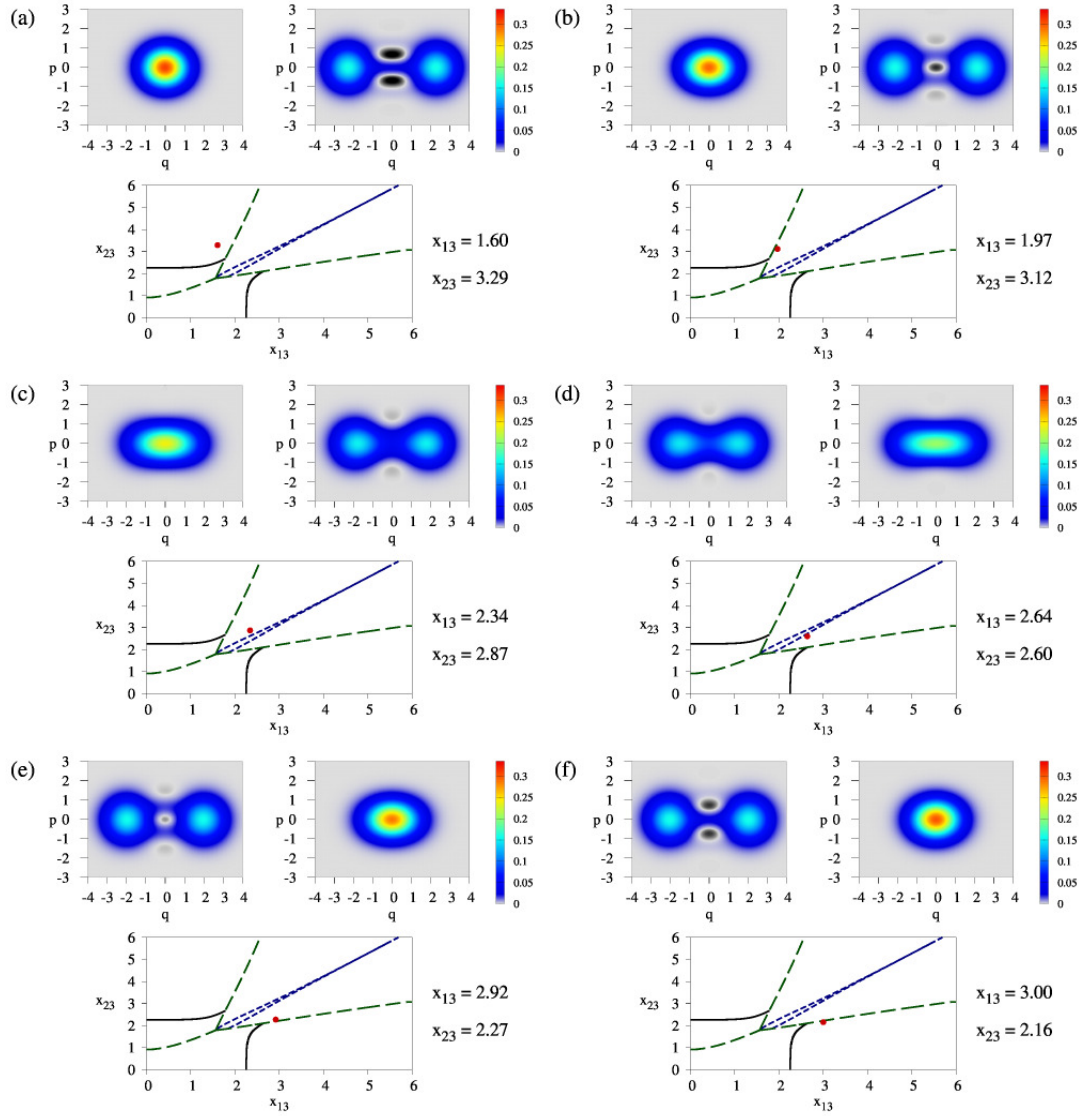


Figure 6. (Colour online) behaviour of the Wigner function close to the normal region as the system goes through different phase transitions: (a)-(b) a discontinuous phase transition $ee \rightleftharpoons oo$, (c)-(d) an unstable-continuous transition, and (e)-(f) a discontinuous transition $oo \rightleftharpoons eo$. The corresponding separatrices according to the type of transition, and the points of calculation (red in the figure), are indicated.

one side of the separatrix to the other, the Wigner function of one mode passes from a circularly symmetric shape to an elongated one along the q -axis, while that of the other mode does the opposite. The fidelity criterion gives us a discontinuous phase transition, since a change of parity occurs. From the Wigner function point of view, the bulk of the ground state changes from a subset of the basis with a major contribution from one kind of photons, to a subset with a major contribution of the other one [compare W_{13} and W_{23} in figures 4(b) and 4(c)]. This behaviour of the Wigner function, which detects this transition in the normal region, reflects the fact that the bulk of the ground

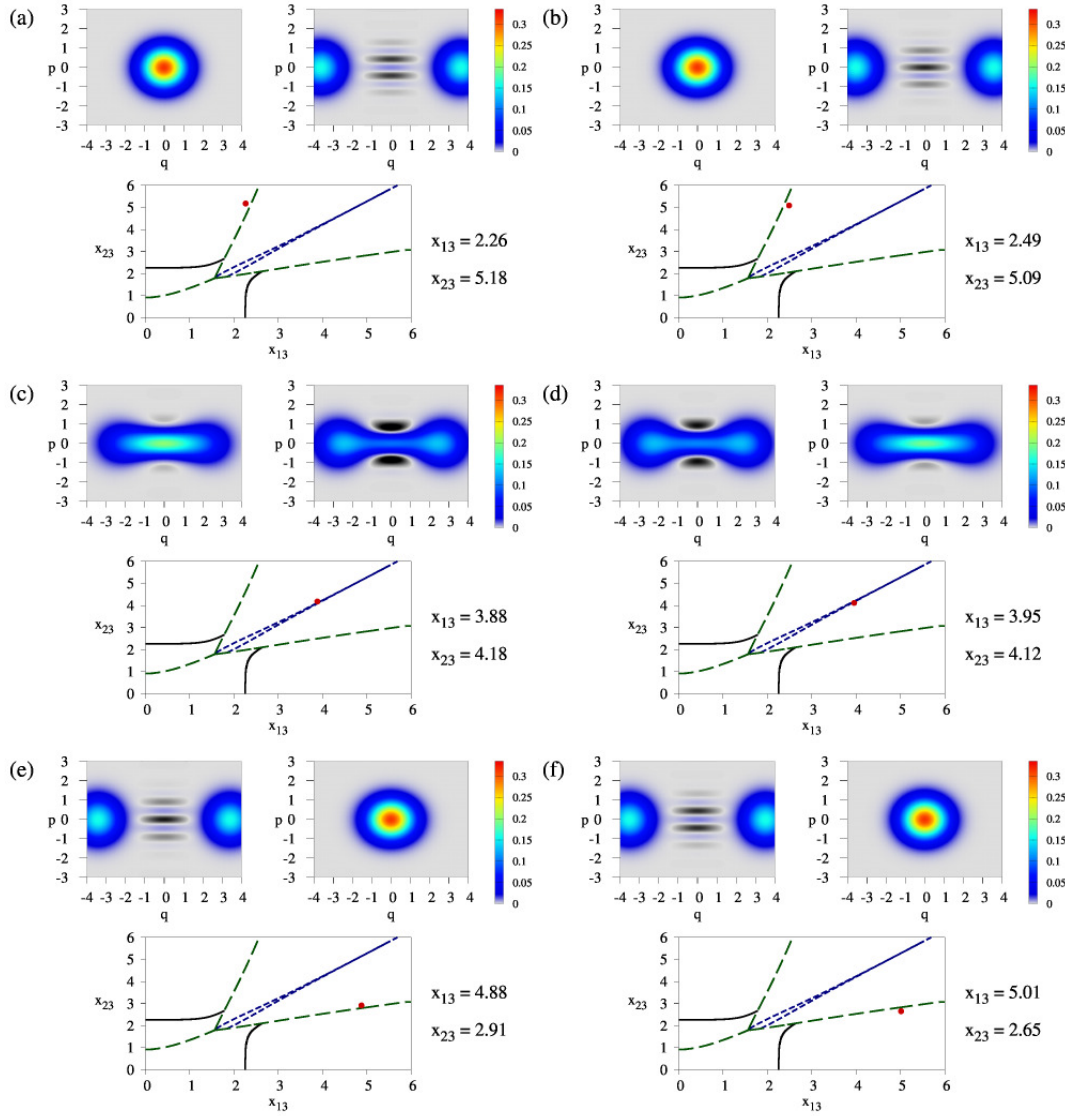


Figure 7. (Colour online) behaviour of the Wigner function for large values of the dipolar strengths, as the system goes through different phase transitions: (a)-(b) a discontinuous transition $ee \rightleftharpoons oo$, (c)-(d) an unstable-continuous transition, and (e)-(f) a discontinuous transition $oo \rightleftharpoons eo$. The corresponding separatrices according to the type of transition, and the points of calculation (red in the figure), are indicated.

state is inside a Hilbert subspace corresponding to a 2-level subsystem, similar to the variational solution.

Fig. 5 depicts the behaviour of the Wigner function as the system goes through a stable-continuous transition (solid line), for small values of x_{23} . In both subregions W_{13} elongates along the q -axis while W_{23} remains without change. (Strictly speaking, the only contribution of field states of mode Ω_{23} is the vacuum). We can see that regions where the Wigner function W_{13} is negative appear as we move away from the normal region and cross the separatrix, a sign of quantumness of the ground state. This

is because the number of photons in mode ν_{13} grows from zero, and we now have a superposition of states with different values of ν_{13} . We will see below that when x_{13} increases, the region between the two main bulks which constitute W_{13} grows as well, and the black (negative valued) regions also grow, reflecting the fact that we have more different values of ν_{13} in superposition. This is a sign of entanglement in the system. Similar results are obtained when the other separatrix (solid line) is crossed (with small values of x_{13} and growing x_{23}); in this case the mode Ω_{23} dominates.

Figures 6 and 7 show, respectively, what occurs when one moves across separatrices in the collective region, for small and large values of the dipolar strengths. In this collective region one finds two discontinuous transitions (dashed lines) due to the change of parity $ee \rightleftharpoons oo$ and $oo \rightleftharpoons eo$ in the ground state, and an unstable-continuous transition (dotted line) which occurs when the state has oo parity [please refer back to Fig. 3(b)].

Discontinuous transition $ee \rightleftharpoons oo$: the Wigner function for the mode Ω_{13} in the collective region ee (above the solid line and to the left of the dashed line) is qualitatively equal to that of the vacuum state, having circular symmetry with positive values, i.e., the contribution of photons ν_{13} is negligible in this region, while the photon contribution ν_{23} is significant, reflected by the fact that W_{23} is very elongated, presenting a bimodal distribution and having negative values (black regions). A similar behaviour of the Wigner function occurs in the region oo once the transition takes place. One may observe that W_{13} does not detect the discontinuous transition $ee \rightleftharpoons oo$, while W_{23} shows a strong change of phase, taking now negative values at the origin [cf. Figs. 6(a)-6(b) and the corresponding Figs. 7(a)-7(b)]. This change of phase in the Wigner function may be seen as a change from a male to a female Schrödinger cat of the field [40].

Unstable-continuous transition [Figs. 6(c)-6(d) and Figs. 7(c)-7(d)]: close to the separatrix in dotted lines both photon contributions are significant. Both Wigner functions present elongated (bimodal) distributions. Above the separatrix the contribution of photons ν_{23} dominates (W_{23} has major regions with negative values), while ν_{13} dominates in the region below the separatrix. The continuous transition is smoother where the separatrix is clearly bifurcated [cf. Figs. 6(c)-6(d)] and more abrupt when it is not [cf. Figs. 7(c)-7(d)]. In both cases, however, when an unstable-continuous transition occurs the field mode contributions to the ground state change their roles.

Discontinuous transition $oo \rightleftharpoons eo$ [Figs. 6(e)-6(f) and Figs. 7(e)-7(f)]: this is the dual of the previous discontinuous transition. The contribution of the mode Ω_{23} is now negligible, while the state of photons of type ν_{13} is the one suffering a change of phase, in a similar fashion to the case of the discontinuous transition $ee \rightleftharpoons oo$ discussed above.

From the results above we see that the Wigner function characterises completely the phase diagram. In the normal region, the Wigner function describes a classical behaviour of the field (W takes positive values) and at least one photon mode remains in the vacuum (cf. Fig. 4). The collective region is characterised by a Wigner function in which the quantumness of the photon modes is clearly shown, or both photon contributions are significant. This latter case occurs close to the unstable-continuous transition (cf. Figs. 6 and 7). In addition, as in the variational solution shown in Fig. 2(b), the

collective region divides itself into two regions, in each of which a single radiation mode dominates.

A video which shows the contour plots of the Wigner functions for the two electromagnetic modes is available online as Supplementary Material [41]. The trajectory in parameter space was chosen to illustrate all the phase transitions, and the behaviour of the system in the various regions.

6. Conclusions

In this paper, we show the results of the characteristics of the ground state for a single three-level atom interacting dipolarly with a two-mode electromagnetic field. The symmetries of the system allow for the division the quantum state space into subspaces which have a well-defined parity with respect to these symmetries, which in turn reduces the dimension of the space considered to calculate the ground state. We have used a fidelity criterion to determine the quantum phase transitions for the three three-level configurations. The phase diagram of the Λ -configuration has the richest structure, and we discuss this case in detail, although the same reasoning can be followed for the other two configurations. To this end, we calculate the Wigner function for each of the electromagnetic modes Ω_{13} and Ω_{23} , and show, in a series of plots, the behaviour of these Wigner functions in the various regions of the parameter space, which supplies further evidence of the quantum phase transitions revealed by the fidelity criterion [26]. One important result is the determination of the regions where the ground state of a single atom in the Λ -configuration shows negative values in the Wigner function, because in these regions the system exhibits a non-classical behaviour. Lastly, a finer classification is proposed for the continuous phase transitions.

Acknowledgments

This work was partially supported by DGAPA-UNAM (under projects IN101619, IN112520, and IN100120).

Appendix A. Surface of Maximum Bures Distance

As pointed out earlier, the phase diagram is determined by the set of points where a minimum of the fidelity between neighbouring states occurs. This quantity depends on one parameter [cf. eq.(8)], i.e., one may consider variations of the fidelity along parametric curves, in parameter space, and determine their local minima; in particular, one may use linear trajectories. A simple test to obtain the phase diagram is to consider trajectories parallel to the axes, and find the set of minima, indicating changes in the ground state at these points. The Wigner function corroborates this by showing changes in the ground state precisely at these points.

In order to obtain a finer description of the phase diagram, however, it is necessary to consider the *surface of minimum fidelity* \mathcal{F}_{\min} or, equivalently, since a minimum value of the fidelity yields also a maximum value of the Bures distance (9), the *surface of maximum Bures distance* $D_{B\max}$. Let $\delta A(\epsilon)$ be the neighbourhood of radius $\epsilon > 0$ about A . Then, at each point A in parameter space, we consider the set of neighbouring points for which a minimum value of the fidelity, or maximum Bures distance is obtained:

$$\mathcal{F}_{\min}(\rho_A, \epsilon) = \min \{ \mathcal{F}(\rho_A, \rho_B) | B \in \delta A(\epsilon) \} . \quad (\text{A.1})$$

$$D_{B\max}(\rho_A, \epsilon) = \max \{ D_B(\rho_A, \rho_B) | B \in \delta A(\epsilon) \} . \quad (\text{A.2})$$

Since constructions (A.1) and (A.2) do not depend on the trajectory, one may obtain a good description of these surfaces by considering sufficient points in $\delta A(\epsilon)$. In our calculation we have taken neighbourhoods of one hundred points, and verified that the qualitative behaviour of the surfaces does not change when taking two hundred points. In addition we have taken radii $\epsilon = 9\delta x/10$ where δx is the minimum distance between the points A that constitute the parameter space (for a regular partition of the parameter space); this selection guarantees to detect any change of the fidelity and Bures distance, and also it does not associate the same value to two neighbouring points in the partition.

The shape of $D_{B\max}$ for the three atomic configurations is shown in Fig. A1. Note that the discontinuities and local maxima correspond perfectly with the separatrices in figure 3. A change of parity in the ground state occurs precisely where these surfaces show discontinuities.

References

- [1] Wigner E 1932 *Phys. Rev.* **40**(5) 749–759
- [2] Hillery M, O’Connell R, Scully M and Wigner E 1984 *Phys. Rep.* **106** 121 – 167 ISSN 0370-1573
- [3] Lee H W 1995 *Phys. Rep.* **259** 147 – 211 ISSN 0370-1573
- [4] Petrucci J C and Alonso M A 2015 *Wigner Function in Optics, The* (American Cancer Society) pp 1–22 ISBN 9783527600441
- [5] Mandel L and Wolf E 1965 *Rev. Mod. Phys.* **37**(2) 231–287
- [6] Barker J and Murray S 1983 *Phys. Lett. A* **93** 271 – 274 ISSN 0375-9601
- [7] Ravaioli U, Osman M A, Ptz W, Kluksdahl N and Ferry D K 1985 *Physica B+C* **134** 36 – 40 ISSN 0378-4363
- [8] Jacoboni C and Bordone P 2004 *Rep. Prog. Phys.* **67** 1033–1071
- [9] Querlioz D, Dollfus P and Mouis M 2013 *Theoretical Framework of Quantum Transport in Semiconductors and Devices* (John Wiley & Sons, Ltd) chap 1, pp 1–56 ISBN 9781118618479
- [10] Mazar R 1998 *Comput. Struct.* **67** 119–124 ISSN 0045-7949
- [11] Kohen D, Marston C C and Tannor D J 1997 *The Journal of Chemical Physics* **107** 5236–5253
- [12] Einstein A, Podolsky B and Rosen N 1935 *Phys. Rev.* **47**(10) 777–780
- [13] Schrödinger E 1935 *Mathematical Proceedings of the Cambridge Philosophical Society* **31** 555–563
- [14] Siyouri F, Baz M E and Hassouni Y 2016 *Quantum Inf. Process.* **15** 4237–4252
- [15] Kenfack A and Życzkowski K 2004 *J. Opt. B: Quantum Semiclass. Opt.* **6** 396–404
- [16] Smithey D T, Beck M, Raymer M G and Faridani A 1993 *Phys. Rev. Lett.* **70**(9) 1244–1247
- [17] Lutterbach L G and Davidovich L 1997 *Phys. Rev. Lett.* **78**(13) 2547–2550

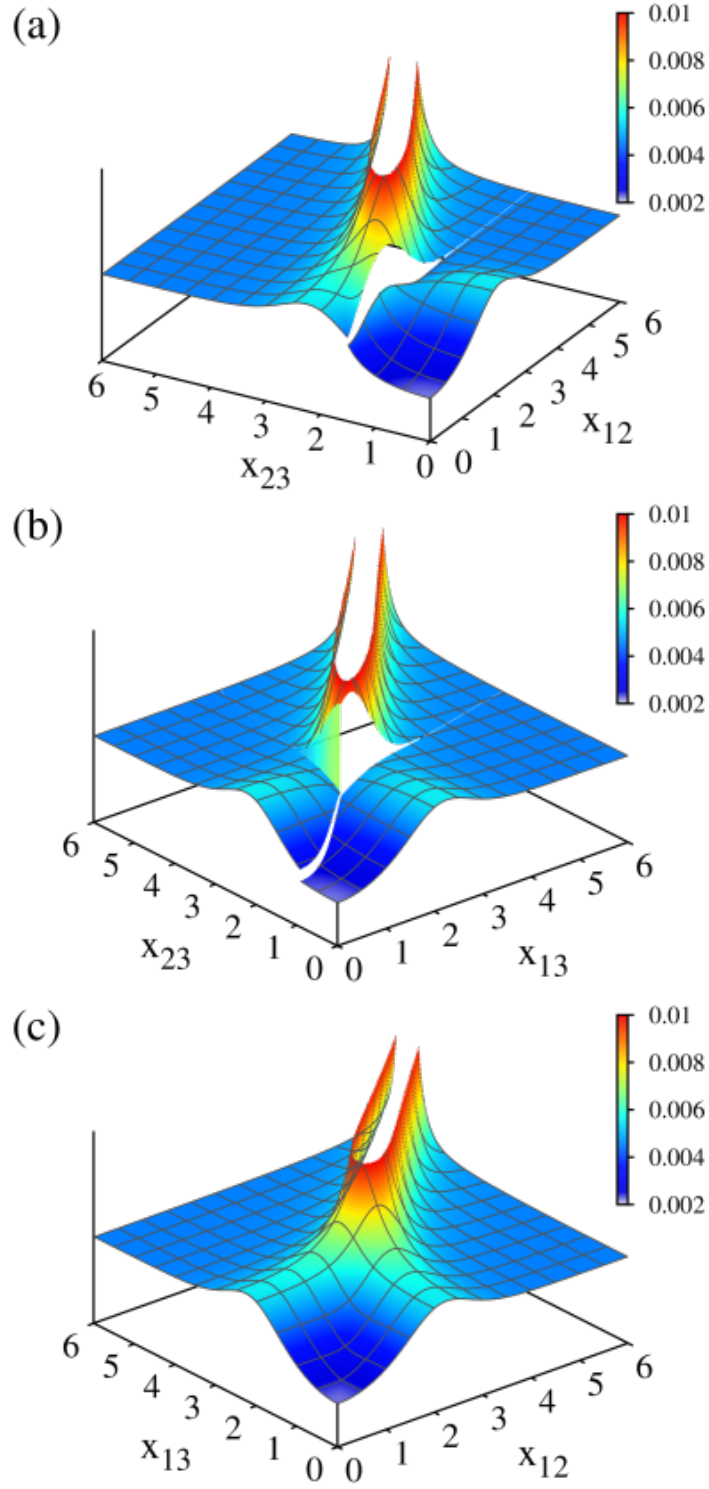


Figure A1. (Colour online) Maximum Bures distance surfaces for the different atomic configurations: Ξ , Λ , V .

- [18] Bertet P, Auffeves A, Maioli P, Osnaghi S, Meunier T, Brune M, Raimond J M and Haroche S 2002 *Phys. Rev. Lett.* **89**(20) 200402
- [19] Banaszek K, Radzewicz C, Wódkiewicz K and Krasinski J S 1999 *Phys. Rev. A* **60**(1) 674–677
- [20] Lee K F, Reil F, Bali S, Wax A and Thomas J E 1999 *Opt. Lett.* **24** 1370–1372
- [21] Mey T, Schfer B and Mann K 2014 *New Journal of Physics* **16** 123042
- [22] Rundle R P, Mills P W, Tilma T, Samson J H and Everitt M J 2017 *Phys. Rev. A* **96**(2) 022117
- [23] Leibfried D, Meekhof D M, King B E, Monroe C, Itano W M and Wineland D J 1996 *Phys. Rev. Lett.* **77**(21) 4281–4285
- [24] Kurtsiefer C, Pfau T and Mlynek J 1997 *Nature* **386** 150153
- [25] Weinbub J and Ferry D K 2018 *Applied Physics Reviews* **5** 041104
- [26] Cordero S, Nahmad-Achar E, López-Peña R and Castaños O Quantum phase diagrams of matter-field hamiltonians i: Fidelity, bures distance, and entanglement arXiv:2002.02491v3 (2020)
- [27] Castaños O, Cordero S, López-Peña R and Nahmad-Achar E 2014 *J. Phys.: Conf. Ser.* **512** 012006
- [28] Cordero S, Nahmad-Achar E, López-Peña R and Castaños O 2015 *Phys. Rev. A* **92**(5) 053843
- [29] Nahmad-Achar E, Cordero S, Castaños O and López-Peña R 2015 *Phys. Scr.* **90** 074026
- [30] Cordero S, Nahmad-Achar E, Castaños O and López-Peña R 2017 *Phys. Scr.* **92** 044004
- [31] Gilmore R 1993 *Catastrophe Theory for Scientists and Engineers* (Dover)
- [32] Cordero S, Castaños O, López-Peña R and Nahmad-Achar E 2019 *Phys. Rev. A* **99**(3) 033811
- [33] Cordero S, Nahmad-Achar E, Castaños O and López-Peña R 2019 *Phys. Rev. A* **100**(5) 053810
- [34] Castaños O, López-Peña R, Nahmad-Achar E and Hirsch J G 2012 *J. Phys. Conf. Ser.* **387** 012021
- [35] Bures D 1969 *Trans. Amer. Math. Soc.* **135** 199–212
- [36] Helstrom C 1967 *Phys. Lett. A* **25** 101–102 ISSN 0375-9601
- [37] Hellmann H Leipzig 1937 *Einführung in die Quantenchemie* (Franz Deuticke)
- [38] Feynman R P 1939 *Phys. Rev.* **56**(4) 340–343
- [39] Castaños O, Cordero S, López-Peña R and Nahmad-Achar E 2018 *Physica Scripta* **93** 085102
- [40] Castaños O, López-Peña R and Man'ko V I 1995 *J. Russ. Laser Res.* **16** 477525
- [41] Videos: contour plots of the Wigner function of the two electromagnetic modes along a path in parameter space [Note to editors, please include here link to the videos]